Applied Catalysis B: Environmental 174–175 (2015) 526–532

Contents lists available at ScienceDirect

Applied Catalysis B: Environmental

journal homepage: www.elsevier.com/locate/apcatb

Morphology-controlled synthesis of ternary Pt–Pd–Cu alloy nanoparticles for efficient electrocatalytic oxygen reduction reactions

Jaeyune Ryu[a,1], Junghun Choi[b,1,2], Dong-Hee Lim[c], Hye-Lin Seo[a], Sang-Young Lee[a,d], Yeonsun Sohn[b], Jin Hoo Park[b], Jong Hyun Jang[a], Hyoung-Juhn Kim[a], Seong Ahn Hong[a], Pil Kim[b,**], Sung Jong Yoo[a,*]

[a] Fuel Cell Research Center, Korea Institute of Science and Technology (KIST), Seoul 136-791, Republic of Korea
[b] School of Semiconductor and Chemical Engineering, Chonbuk National University, Jeonju 561-756, Republic of Korea
[c] Department of Environmental Engineering, Chungbuk National University, Cheongju 362-763, Republic of Korea
[d] Department of Fusion Chemical Engineering, Hanyang University, Ansan 426-791, Republic of Korea

ARTICLE INFO

Article history:
Received 2 October 2014
Received in revised form 11 February 2015
Accepted 12 March 2015
Available online 14 March 2015

Keywords:
Oxygen reduction reaction
Electrocatalysis
Ternary alloy nanoparticles
Morphology control
Galvanic displacement reaction

ABSTRACT

In the present work, we have accomplished morphology-controlled synthesis of ternary Pt–Pd–Cu alloy nanoparticles, particularly for efficient electrocatalytic oxygen reduction reactions. By controlling over the degree of galvanic displacement at room temperature, we selectively introduced porous and hollow architectures into Pt-decorated Pd–Cu alloy nanoparticles. Porous morphology was accompanied with partially facilitated Pt substitution reaction while hollow shape was exclusively achieved when the galvanic reaction was coupled with additional pre-treatment process which could eventually make the following displacement reaction more facile. Not only the both porous and hollow Pt@PdCu/C catalysts exhibited enhanced ORR performances compared to commercial Pt/C, but also they displayed outstanding durability. In addition, we investigated the alloying effects between Pt and Pd–Cu composite and the presumable influences of lattice strain through preliminary theoretical calculation to account for the enhanced ORR efficiency and durability of the present catalysts.

1. Introduction

The investigation of highly active and stable catalysts for cathodic oxygen reduction reaction (ORR) has been widely pursued for the application of proton-exchange-membrane fuel cells (PEMFCs). Nonetheless, overcoming sluggish oxygen reduction kinetics with a minimum amount of expensive and scarcely available Pt is still considered as a critical hurdle for the widespread commercialization of the PEMFC technology [1–4].

Along with considerable efforts in theoretical designs and experimental validations, several mechanism-based strategies have been established for enhancing ORR activity while reducing Pt usage [1–6]. Pt skin formation [7–13], lattice contraction [14–17], and modification of d-band center of Pt can be critical examples [18–22]. Accordingly, alloying Pt with first-row transition metals (V, Cr, Mn, Fe, Co, Ni, and Cu) or early transition metals (Hf, La, Sc, and Y) has been actively studied [1–6,18–27]. In particular, introduction of Pt monolayers (core-shell structure) by the displacement of underpotential-deposited (UPD) Cu on different substrates were revealed to exhibit significantly increased Pt-mass activities [9–13]. Furthermore, selective formation of Pt-rich shells surrounding an alloy core through de-alloying process has successfully resulted in high mass activities of Pt in the presence of compressive strains which found to play a dominant role in ORR electrocatalysis [15–17].

Inspired by above mentioned aspects, we envisioned to develop a novel ternary alloy system along with facile control of the nanoparticle morphology [28–30]. We basically targeted the ternary Pt–Pd–Cu composite since it has been evaluated as promising for ORR. With different synthetic approaches, several groups including us have independently explored core-shell type $Pt@Pd_xCu_y/C$ electrocatalysts for ORR and methanol oxidation [31–35]; however, studies relate to morphology control of the ternary system and its applications for ORR have rarely been achieved. Herein, we report morphology-controlled synthesis of

* Corresponding author. Tel.: +82 29585260.
** Corresponding author.
E-mail addresses: kimpil1@chonbuk.ac.kr (P. Kim), ysj@kist.re.kr (S.J. Yoo).
[1] Both authors contributed equally to this work.
[2] Present address: Future Technology Research Center, Corporation R&D, Research Park, LG Chem, Daejeon 305-738, Republic of Korea.

http://dx.doi.org/10.1016/j.apcatb.2015.03.019
0926-3373/

ternary Pt–Pd–Cu alloy nanoparticles through room temperature galvanic displacement reactions. By controlling over the degree of galvanic substitution under the mild condition, we selectively introduced porous and hollow architectures into Pt-decorated Pd–Cu alloy nanoparticles. The as-resultant porous and hollow ternary alloy nanoparticles on carbon support exhibited higher oxygen reduction activities and durability compared to those of commercial Pt/C. Our preliminary theoretical model studies also well validated the experimental demonstrations by dealing with oxygen binding energy and vacant formation energy of Pt in the present catalysts.

2. Experimental

2.1. Catalyst synthesis

2.1.1. Preparation of 20 wt% $PdCu_3$/C

Mixture of palladium (II) nitrate hydrate ($Pd(NO_3)_2{\cdot}2.3H_2O$, KOJIMA Chemicals, 0.25 mmol), copper (II) nitrate ($Cu(NO_3)_2{\cdot}3H_2O$, Shinyo Pure Chemicals, 0.76 mmol) and carbon black (Vulcan XC-72R, Cabot, 0.3 g) in 150 mL triply distilled DI water was stirred vigorously for 30 min and subsequently ultrasonificated for 40 min. To the mixture, sodium borohydride ($NaBH_4$, Aldrich, 4.1 mmol) in 25 mL DI water was added dropwisely (5 mL min^{-1}). Then, the final reaction mixture was stirred for 1 h at room temperature and washed by filtration with excessive DI water (2L). The as-prepared $PdCu_3$/C was dried in convection oven for overnight at 100 °C. Lastly, high temperature heat treatment process under N_2 atmosphere was performed to clean the surface of absorbed byproducts, further alloy the bimetallic particles, and afford Cu-rich surface. The annealing temperature was elevated from 20 to 600 °C with continuous rate 1.5 °C min^{-1}, and then was kept at 600 °C for 1 h. After that, the temperature was slowly cooled to 20 °C in the furnace.

2.1.2. Preparation of porous Pt@PdCu/C

Mixture of $PdCu_3$/C (0.1 g) in N_2 purged (30 min) triply distilled DI water (100 mL) was stirred vigorously for 30 min and subsequently ultrasonificated for 30 min. After the reaction mixture was additionally recharged with N_2 gas for 20 min, N_2 purged solution of hydrogen hexachloroplatinate in triply distilled water (20 mL, 3.3 mM) was added dropwisely to the mixture (1.6 mL min^{-1}). After the addition, the final reaction mixture was stirred for 2 h under N_2 atmosphere and washed by filtration with excessive DI water (2L). The as-resultant porous Pt@PdCu/C was dried in convection oven for overnight at 100 °C.

2.1.3. Preparation of hollow Pt@PdCu/C

Mixture of $PdCu_3$/C (0.1 g) in N_2 purged (30 min) triply distilled DI water (100 mL) was stirred vigorously for 30 min and subsequently ultrasonificated for 30 min. Before directly applying the galvanic displacement condition, the mixture was heated to 100 °C by 2.5 °C min^{-1} rate and maintained for 3 h under continuous H_2 purging. After the pre-treatment, the reaction mixture was cooled to room temperature and N_2 gas was recharged for 20 min. And then, N_2 purged solution of hydrogen hexachloroplatinate ($H_2PtCl_6{\cdot}5.6H_2O$, KOJIMA Chemicals) in triply distilled water (20 mL, 3.3 mM) was added dropwisely to the mixture (1.6 mL min^{-1}). After the addition, the final reaction mixture was stirred for 2 h under N_2 atmosphere and washed by filtration with excessive DI water (2L). The as-resultant hollow Pt@PdCu/C was dried in convection oven for overnight at 100 °C.

2.2. Electrochemical characterization

All electrochemical measurements were conducted in a standard three-compartment electrochemical cell. Pt gauze and Ag/AgCl (Cl^- saturated) were used as counter and reference electrodes, respectively. A working electrode was constructed with a catalyst-ink coated rotating disk electrode (disk diameter: 5.61 mm, Pine Research Instrumentation). The catalyst ink was prepared by the method reported in the literature [36] and amount of catalyst loading on the disk electrode was 15 $\mu g_{(PGM,Pt+Pd)}$ cm^{-2}. All measurements were reported versus reversible hydrogen electrode (RHE). The RHE calibration was performed in hydrogen saturated electrolyte with a Pt electrode as the working electrode. The potential at which the current crossed zero was taken to be the thermodynamic potential for the hydrogen electrode reactions.

For the evaluation of the ORR performance, linear sweep voltammetry was carried out in the potential range of 0.315–1.115 V (vs RHE) at a weep rate of 10 mV s^{-1} with a rotation rate of 1600 rpm in O_2 saturated 0.1 M $HClO_4$ solution. Cyclic voltammetry (CV) was performed in the potential range of 0.05–1.2 V (vs RHE) at a scan rate of 100 mV s^{-1} in N_2 purged 0.1 M $HClO_4$ solution. The electrochemical surface area (ESA) is determined by integrating the anodic curve from 0.05 to 0.4 V after subtracting the double-layer capacitance and applying a charge density of 210 $\mu C\,cm^{-2}$ for the under potential deposition (UPD) of hydrogen. The accelerated degradation tests (ADT) were performed in order to measure the durability of the present hollow and porous Pt@PdCu/C as well as commercial Pt/C (20 wt%, Johnson Matthey). After the potential cycling of 10,000 times (scan rate = 100 mV s^{-1}) between 0.60 and 1.00 V with rotating speed of 1600 rpm, the CV and ORR tests were repeated in 0.1 M $HClO_4$.

2.3. Physical characterization

The particle distribution and size of the prepared cobalt based catalysts were investigated by (high resolution) transmission electron microscopy (JEM-ARM200F, JEOL). The chemical distribution of the present cobalt based nanoparticles was examined using scanncing transmission electron microscopy (STEM) and energy dispersive x-ray spectroscopy (EDX) (H-7650, Hitachi). Inductively coupled plasma-optical emission spectroscopy (ICP-OES) (US EPA 3050B, PerkinElmer) was performed to confirm the weight percent of each metal on the catalysts. By X-ray diffraction (XRD) (Rigaku, D/MAX 2500) with Cu Kα radiation operated at 40 kV and 30 mA, the diffraction patterns of catalysts were obtained in 2 theta ranges between 10 and 80° with scanning speed, 6° min^{-1}.

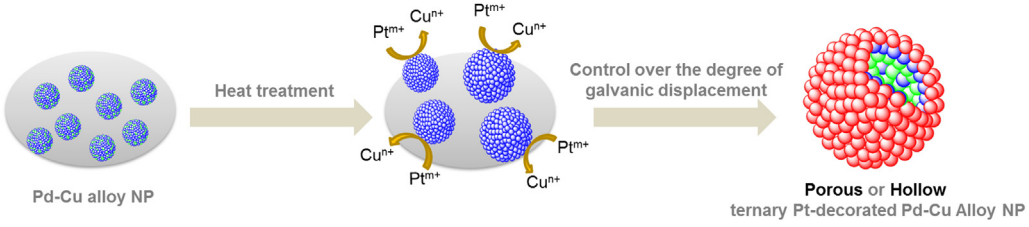

Scheme 1. A schematic illustration for the synthetic procedures of the present catalysts (carbon black support is omitted in the picture for simplicity).

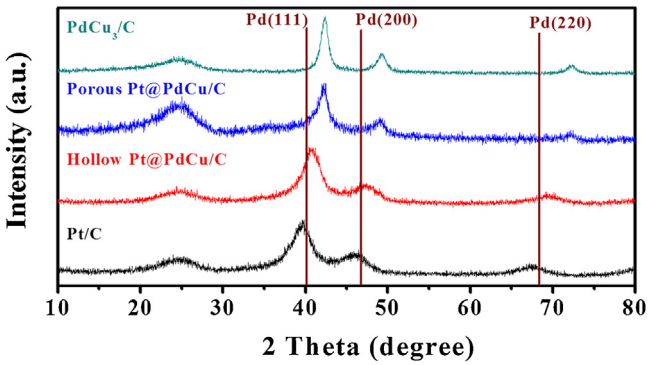

Fig. 1. XRD spectra of $PdCu_3$/C, porous Pt@PdCu/C, hollow Pt@PdCu/C, and commercial Pt/C.

3. Results and discussion

The synthetic procedure of the present catalysts is depicted in Scheme 1. $PdCu_3$ alloy nanoparticles deposited on carbon black support (Vulcan XC-72) were firstly synthesized by borohydride reduction followed by high-temperature heat treatment (600 °C) (Fig. S1). Chemical composite of the as-resultant spherical shaped $PdCu_3$ nanoparticles (~9.2 nm) was unambiguously confirmed by XRD (Fig. 1), EDX (Fig. S2), and ICP analysis (Table S1). Overall positive peak shifts relative to pure palladium phase clearly show the successful alloy between palladium and copper. Lack of hydrogen UPD in the initial cyclic voltammogram of $PdCu_3$/C indicates Cu-richness of the surface of $PdCu_3$ nanoparticles (Fig. S3).

The outer Pt shell was introduced by galvanic displacement between Cu species at the surface of $PdCu_3$ nanoparticles and Pt ions in water solution. It is highly likely that Pt ions with higher reduction potentials than that of Cu^{2+}/Cu^0 would replace Cu atoms

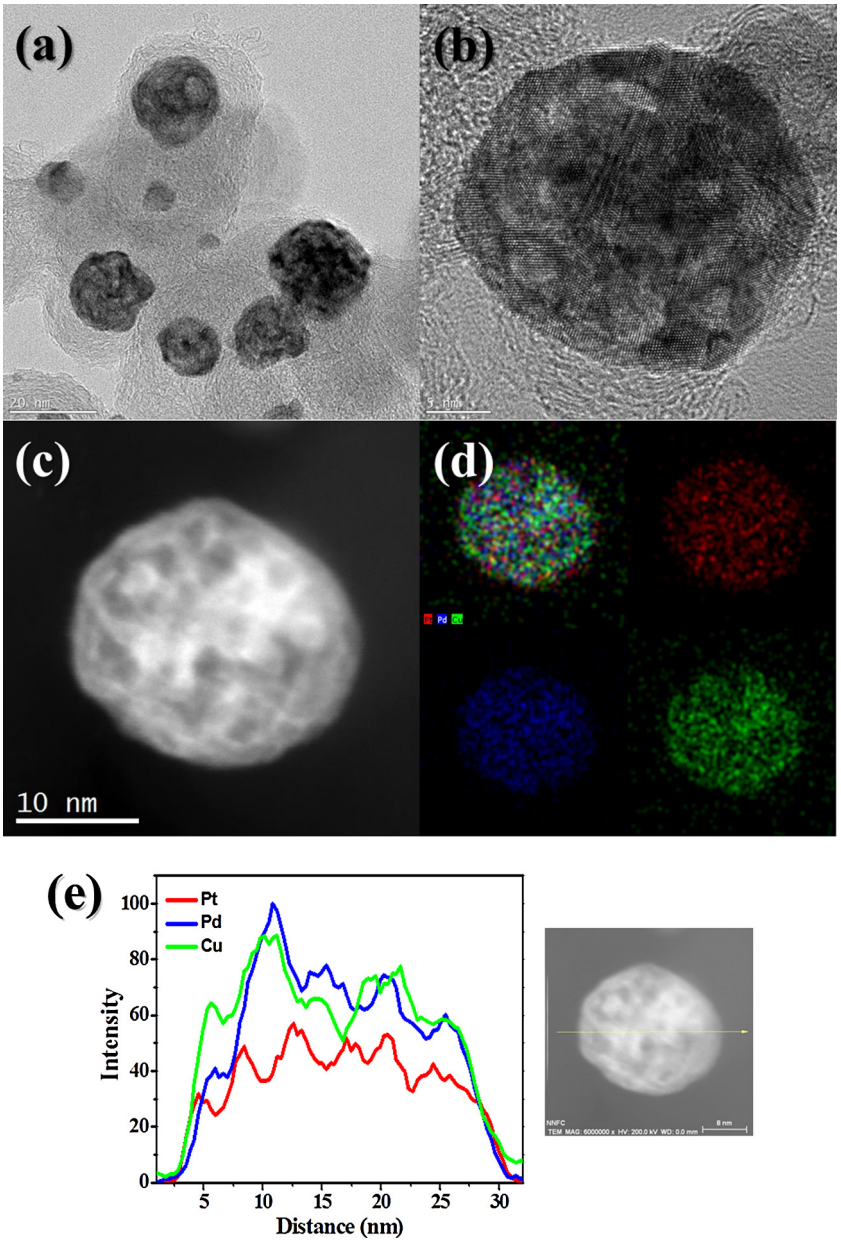

Fig. 2. (a) TEM, (b) HR-TEM, and (c) STEM images of porous Pt@PdCu/C. (d) EDX mapping (red for Pt, blue for Pd, and green for Cu), and (e) EDX line profiling data of a porous Pt@PdCu nanoparticle.

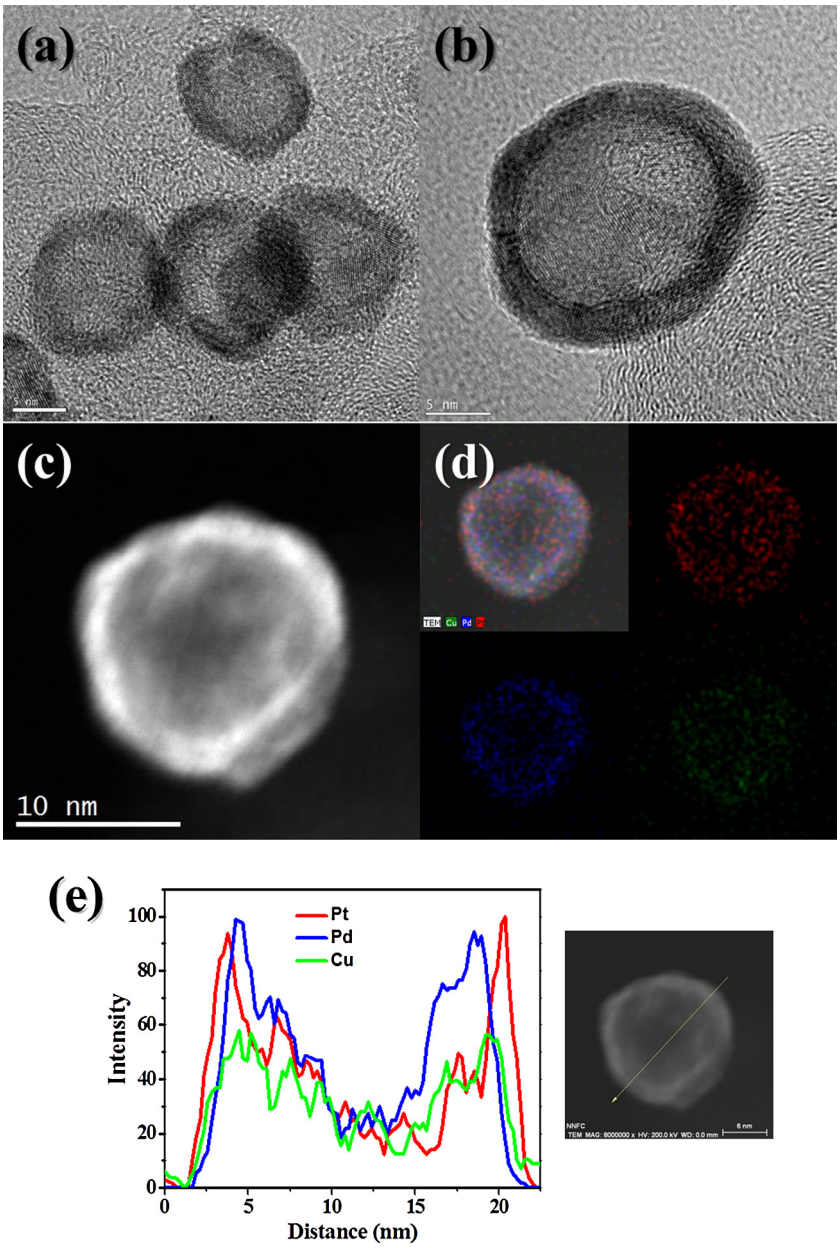

Fig. 3. (a) TEM, (b) HR-TEM, and (c) STEM images of hollow Pt@PdCu/C. (d) EDX mapping (red for Pt, blue for Pd, and green for Cu), and (e) EDX line profiling data of a hollow Pt@PdCu nanoparticle. (For interpretation of the references to colour in this figure legend, the reader is referred to the web version of this article.)

spontaneously. According to the reduction potential values, the displacement of Cu by Pt ions will be more favorable thermodynamically and kinetically in comparison to the reaction between Pd and Pt ions [31–34]. Directly applied galvanic reaction under the room engendered Pt incorporated ternary nanoparticles with unique irregular nanoporosity (as-resultant sample is denoted as porous Pt@PdCu/C, Fig. 2), as revealed in the (high resolution) TEM images. Atomic distribution of Pt, Pd, and Cu was also scrutinized by EDX-mapping and line profiling analysis (Fig. 2). Meanwhile, slight negative shift from $PdCu_3$ phase in X-ray diffraction (0.2–0.3°) indicates that small amount of Pt atoms are introduced under the replacement reaction (Fig. 1). Additionally, low weight contents of the incorporated Pt (less than 4%) (Table S1) as well as evident Cu dissolution peaks detected at the initial CV scanning (Fig. S3) for the porous Pt@PdCu/C imply the formation of incomplete or sub-monolayer Pt shells during the galvanic reaction [32,33]. Besides, we have conduced XPS analysis to check the state of Pt for the present catalysts. As you can see in Figure S4, contribution of Pt (II) species is remarkable in the XPS spectrum of the porous catalyst. This result suggests that Pt of the porous nanoparticles bear exclusive surficial nature with the lack of bulk composite, consistent with the features of incomplete or sub-monolayered shell-like architectures [37].

On the other hand, when the galvanic displacement reaction was coupled with additional pre-treatment process in which $PdCu_3$/C in water solution was stirred at 100 °C under continuous H_2 purging, the subsequently conduced Pt substitution at room temperature provides complete Pt outer shells along with exclusive nano-hollow morphology (As-resultant sample is denoted as hollow Pt@PdCu/C, Fig. 3). The hollow architectures of resulting nanoparticles were ascertained through high resolution TEM, STEM, and EDX analysis (Fig. 3). Particularly, outer location of the substituted Pt is clearly shown by the EDX line profile (Fig. 3e). Compared to the already described porous Pt@PdCu/C, hollow Pt@PdCu/C exhibited larger

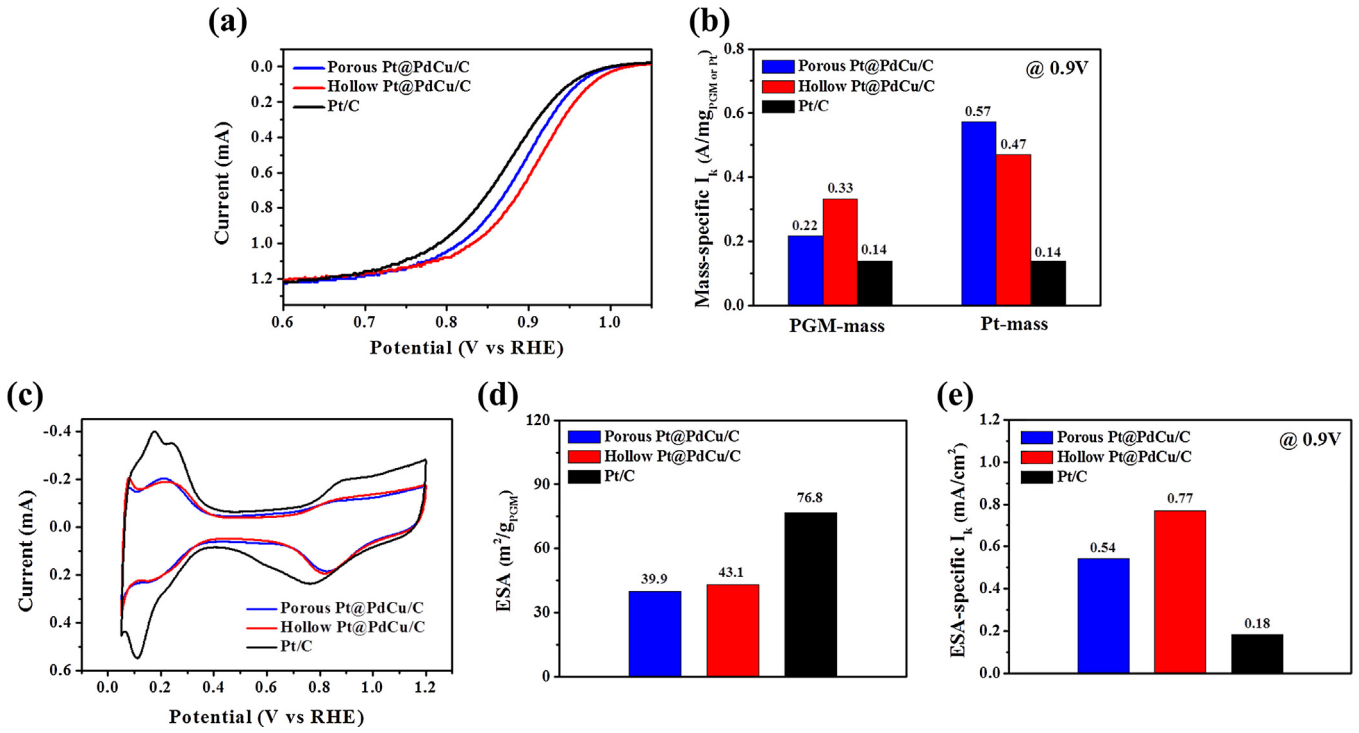

Fig. 4. (a) ORR Polarization curves obtained with a rotation rate of 1600 rpm and a sweep rate of 10 mV s^{-1}. The catalyst loading on the disk electrode was 15 μg_{PGM} cm^{-2}. (b) Mass-specific kinetic currents at 0.9 V of present catalysts and commercial Pt/C. (c) Cyclic voltammograms measured with a seep rate of 100 mV s^{-1} in N_2-purged 0.1 M $HClO_4$ solution. (d) ESA values and (e) ESA-specific kinetic currents at 0.9 V of present catalysts and commercial Pt/C.

weight percent of Pt (13%, table S1) and clear negative shifts in X-ray diffraction, indicating that more complete Pt-substitution with a certain amount of inter-diffusion or alloying near the interface between the core and the shell was taken place. Besides, no detectable Cu dissolution peak at initial CV of hollow Pt@PdCu/C implies complete Pt-shell formation around the core Pd–Cu composite, which is in contrast to the case of porous Pt@PdCu/C (Fig. S3).

The formation of porous or hollow structures would be governed by galvanic displacement reaction and nanoscale kirkendall effect. The driving force for the galvanic displacement is the difference of reduction potentials between two metals while the net flux of compensating vacancies is proportional to the diffusivity difference in the kirkendall diffusion process [38–40]. Since Pt diffuses slower than Cu and Pd, vacancies will be generated inside the core-shell nanostructures, and they will coalesce into a single void (hollow) or multiple void (porous) depending on the reaction conditions. Unlike uniformly proceeded galvanic reaction, partial displacement at the surface may generate irregular multiple void (porosity), which couldn't be integrated into one big void to form hollow architectures. Particularly, surficial composites of copper in the template $PdCu_3$ particles are believed to affect the degree of galvanic displacement reaction and eventually influence the final morphologies of ternary alloy nanoparticles. In order to validate this aspect, we have conducted ex-situ XPS analysis for the template material, $PdCu_3$/C, before and after applying the pre-treatment process. (Figure S5). As you can see in Figure S5, the pre-treatment greatly changed the surface composites of copper. The increased shoulder features in Cu $2P_{3/2}$ peak (~934.3 eV) indicates increased $Cu(OH)_2$ species at the surface. Even though the as-resultant XPS results can not represent the exact in-situ state of copper composites since our analysis was performed in ex-situ manner (The recovered sample from the pre-treatment would be directly oxidized by air contact before analysis.), the results clearly imply that the pre-treatment induces significant changes in the composite of copper species at the surface of $PdCu_3$ nanoparticles. More detail mechanistic investigation is now underway in our laboratory.

Next, electrocatalytic ORR performances of the present materials were evaluated (Fig. 4). Fig. 4a shows ORR polarization curves of the porous and hollow Pt@PdCu/C as well as commercial Pt/C (20 wt%, Johnson Matthey) deposited onto a glassy carbon working electrode (loading: 15 μg_{PGM} cm^{-2}), measured on a rotating disk electrode (RDE) in 0.1 M $HClO_4$ solution at 25 °C. In addition to the polarization curves, kinetic currents at 0.9 V were considered to compare the ORR activities of the present catalysts more precisely. To our delight, both hollow and porous Pt@PdCu/C exhibited ~0.90 V and ~0.88 V of half-wave potentials, respectively, which are ~40 mV and ~20 mV larger values than that of commercial Pt/C (~0.86 V). The calculated mass-specific kinetic currents based on the polarization curves clearly notified the enhanced ORR activities of the present catalysts compared to commercial Pt/C (Fig. 4b). In terms of PGM-mass, the mass specific activities of the hollow and porous Pt@PdCu/C are 0.33 A mg_{PGM}^{-1} and 0.22 A mg_{PGM}^{-1}, respectively, which are 2.4- and 1.6-fold enhanced values relative to that of commercial Pt/C (0.14 A mg_{Pt}^{-1}). When considering the Pt-mass only, the hollow and porous Pt@PdCu/C displayed 3.4- and 4.1-fold enhanced mass activities (0.47 A mg_{Pt}^{-1} and 0.57 A mg_{Pt}^{-1}) which both surpass the 2017 DOE mass activity target (0.44 A mg_{Pt}^{-1}). The large discrepancy between PGM-based and Pt-based mass activities of porous Pt@PdCu/C originated from its low Pt/Pd mass ratio.

Meanwhile, the electrochemical surface areas (ESA) of the present catalysts and commercial Pt/C were calculated by integrating hydrogen desorption charges based on the CV data (Fig. 4c). Both hollow and porous Pt@PdCu/C catalysts have similar ESA values (~40 m^2 g_{PGM}^{-1}) which are smaller than that of commercial Pt/C (77 m^2 g_{PGM}^{-1}) probably due to their relatively large particle sizes mainly (Fig. 4d). Even though ESA values themselves might be considered to understand the relative trend because

the presence of Pd on the Pt@PdCu/C surface could influence the estimation, the ESA-specific activities of the hollow and porous Pt@PdCu/C are revealed as 0.77 mA cm^{-2} and 0.54 mA cm^{-2} at 0.9 V, respectively, which are 4.3- and 3.0-fold enhanced activities relative to that of commercial Pt/C (0.18 mA cm^{-2}) (Fig. 4e). The large ESA-specific activity of the hollow Pt@PdCu/C, which also exceeds 2017 DOE target (0.72 mA cm^{-2}), may be attributed to its innate morphological advantages in addition to alloying effects. Furthermore, the present hollow and porous Pt@PdCu/C catalysts also displayed outstanding stability (Fig. 5). Durability of the catalyst was tested by cycling the potential between 0.6 V and 1.0 V (vs RHE) at 100 mV s^{-1} in O_2 saturated 0.1 M $HClO_4$ (Fig. S4). During the 10,000 cycles, commercial Pt/C experienced 25% deduction of ESA while both hollow and porous Pt@PdCu/C catalysts only recorded ~12% loss (Fig. 5a). Besides, the percentages of kinetic current loss (at 0.9 V) of the present catalysts (12% for hollow catalyst and 10% for porous catalyst) are less than the half of the deterioration that commercial Pt/C experienced (27%) (Fig. 5b). The desirable stability of hollow and porous Pt@PdCu/C is likely due to the alloying effects between Pt and Pd–Cu composite, in addition to their large particle size.

As mentioned, the enhanced ORR performances of the present hollow and porous Pt@PdCu/C can be primarily ascribed to the alloying effects between Pt and Pd–Cu composite. On the experimental basis, electronic structure modification of surficial Pt was ascertained by CV (Fig. 4c) in which the present Pt@PdCu/C catalysts show evident positive shifts (~60 mV) in the oxide reduction peak (0.82–0.83 V) with respect to Pt/C (0.76 V). The large positive shifts of the oxide reduction peak indicate electronic structure alterations of Pt to afford delay in the onset of Pt–OH formation, which closely links to the improved ORR rate [1,10,18–22]. In accordance with the experimental evidence, our preliminary theoretical studies also verified the influence of Pd–Cu composite onto Pt (Fig. 6). According to our DFT calculations, the underneath Pd–Cu composite can lower the oxygen adsorption energies of surficial Pt, which is believed to be a key factor for the improved ORR activities of the present catalysts. The hollow site of Pt (1 1 1)@PdCu in our model structure

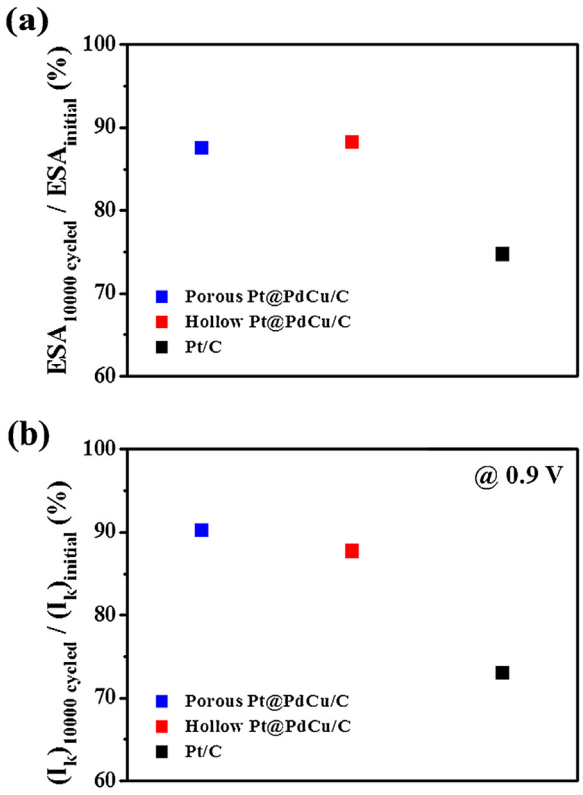

Fig. 5. Durability of the present catalysts and commercial Pt/C in terms of ESA values and kinetic currents at 0.9 V. The comparison was made by considering those measured before and after 10,000 potential cycling.

(Fig. 6a) displayed lowered oxygen adsorption energy compared to that of Pt (1 1 1) (Fig. 6b, see the supporting information for details). Since the ORR rate at high potentials is hampered by the steps including desorption of O and OH reaction intermediates, weakening the strength of oxygen binding has been known for an effective

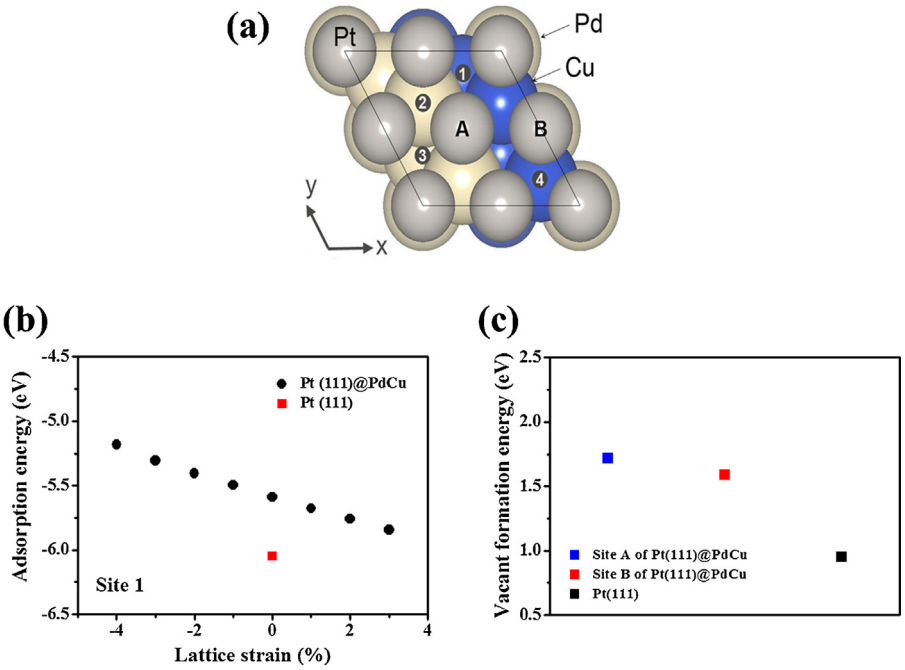

Fig. 6. (a) The model structure representing Pt (1 1 1) mono layer onto the Pd–Cu composite. (b) Oxygen adsorption energy of Pt (1 1 1) and Pt (1 1 1) over Pd–Cu composite and its dependence to lattice strains. See the supporting information for details. (c) The comparison for vacant formation energies of bare Pt (1 1 1) and Pt (1 1 1) over Pd–Cu composite.

way of increasing the ORR kinetics [1–6,14–22]. Increasing vacant formation energy (which is regarded as a useful descriptor for the stability) of Pt in the ternary system can also explain the improved durability of the present alloy catalysts (Fig. 6c). Besides, supplement calculations revealed that oxygen binding energy become further weakened as compressive (negative) strains are imposed to Pt on Pd–Cu composite (Fig. 6b). The result implies that high ORR specific activity of hollow Pt@PdCu/C can be additionally attributed to the presumable lattice contraction induced by the hollow morphology [40].

4. Conclusion

So far, we have described novel ternary Pt–Pd–Cu alloy nanoparticular systems for effective oxygen reduction reactions. Control over the degree of galvanic replacement allowed the morphology-controlled synthesis of Pt@PdCu ternary nanoparticles. To our delight, both porous and hollow Pt@PdCu/C catalysts showed enhanced ORR activities as well as outstanding durability compared to commercial Pt/C. Our preliminary theoretical model studies also verify the experimental results by elucidating alloying effects and influences of lattice strain in the present ternary catalytic systems.

Acknowledgements

This research was supported financially by Global Frontier R&D Program on Center for Multiscale Energy System (NRF-2012-M3A6A7054283), the NRF grant funded by MSIP (2014-R1A2A2A04003865), the KIST Institutional Program of Korea Institute of Science and Technology (KIST), the New and Renewable Energy Core Technology Program of KETEP grant funded by MOTIE (2013-3030011320) and Basic Science Research Program (NRF-2012R1A6A3A04040490).

Appendix A. Supplementary data

Supplementary data associated with this article can be found, in the online version, at http://dx.doi.org/10.1016/j.apcatb.2015.03.019.

References

[1] H.A. Gasteiger, S.S. Kocha, B. Sompalli, F.T. Wagner, Appl. Catal. B: Environ. 56 (2005) 9–35.
[2] H.A. Gasteiger, N.M. Markovic, Science 324 (2009) 48–49.
[3] V. Stamenkovic, B.S. Mun, M. Arenz, K.J.J. Mayerhofer, C.A. Lucas, G. Wang, P.N. Ross, N. Markovic, Nat. Mater. 6 (2007) 241–247.
[4] V.R. Stamenkovic, B. Fowler, B.S. Mun, G. Wang, P.N. Ross, C.A. Lucas, N.M. Markovic, Science 315 (2007) 493–497.
[5] M.K. Debe, Nature 486 (2012) 43–51.
[6] N. Jung, D.Y. Chung, J. Ryu, Y.-E. Sung, S.J. Yoo, Nano Today 9 (2014) 433–456.
[7] T. Toda, H. Igarashi, M. Watanabe, J. Electroanal. Chem. 460 (1999) 258–262.
[8] V.R. Stamenkovic, B.S. Mun, K.J.J. Mayrhofer, P.N. Ross, N.M. Markovic, J. Am. Chem. Soc. 128 (2006) 8813–8819.
[9] R.R. Adzic, J. Zhang, K. Sasaki, M.B. Vukmirovic, M. Shao, J.X. Wang, A.U. Nilekar, M. Mavrikakis, J.A. Valerio, F. Uribe, Top. Catal. 46 (2007) 249–262.
[10] J. Zhang, Y. Mo, M.B. Vukmirovic, R. Klie, K. Sasaki, R.R. Adzic, J. Phys. Chem. B 108 (2004) 10955–10964.
[11] W.P. Zhou, X. Yang, M.B. Vukmirovic, B.E. Koel, J. Jiao, G. Peng, M. Mavrikakis, R.R. Adzic, J. Am. Chem. Soc. 131 (2009) 12755–12762.
[12] T. Ghosh, M.B. Vukmirovic, F.J. DiSalvo, R.R. Adzic, J. Am. Chem. Soc. 132 (2010) 906–907.
[13] K. Sasaki, H. Naohara, Y.M. Choi, Y. Cai, W.-F. Chen, P. Liu, R.R. Adzic, Nat. Commun. 3 (2012) 1115.
[14] S. Mukerjee, S. Srinivasan, M.P. Soriaga, J. McBreen, J. Electrochem. Soc. 142 (1995) 1409–1422.
[15] S. Koh, P. Strasser, J. Am. Chem. Soc. 129 (2007) 12624–12625.
[16] R. Strivastava, P. Mani, N. Hahn, P. Strasser, Angew. Chem. Int. Ed. 46 (2007) 8988–8991.
[17] P. Strasser, S. Koh, T. Anniyev, J. Greeley, K. More, C. Yu, Z. Liu, S. Kaya, D. Nordlund, H. Ogasawara, M.F. Toney, A. Nilsson, Nat. Chem. 2 (2010) 454–460.
[18] J.K. Nørskov, J. Rossmeisl, A. Logadottir, L. Lindqvist, J.R. Kitchin, T. Bligaard, H. Jonsson, J. Phys. Chem. B 108 (2004) 17886–17892.
[19] V.S. Murthi, R.C. Urian, S. Mukerjee, J. Phys. Chem. B 108 (2004) 11011–11023.
[20] J. Zhang, M.B. Vukmirovic, Y. Xu, M. Mavrikakis, R.R. Adzic, Angew. Chem. Int. Ed. 44 (2005) 2132–2135.
[21] J. Greeley, I.E.L. Stephens, A.S. Bondarenko, T.P. Johansson, H.A. Hansen, T.F. Jaramillo, J. Rossmeisl, I. Chorkendorff, J.K. Nørskov, Nat. Chem. 1 (2009) 552–556.
[22] V. Stamenkovic, B.S. Mun, K.J.J. Mayrhofer, P.N. Ross, N.M. Markovic, J. Rossmeisl, J. Greeley, J.K. Norskov, Angew. Chem. Int. Ed. 45 (2006) 2897–2901.
[23] Y. Bing, H. Liu, L. Zhang, D. Ghosh, J. Zhang, Chem. Soc. Rev. 39 (2010) 2184–2202.
[24] T. Toda, H. Igarashi, H. Uchida, M. Watanabe, J. Electrochem. Soc. 146 (1999) 3750–3756.
[25] I.E.L. Stephens, A.S. Bondarenko, U. Grønbjerg, J. Rossmeisl, I. Chorkendorff, Energy Environ. Sci. 5 (2012) 6744–6762.
[26] S.J. Yoo, S.J. Hwang, J.-G. Lee, S.-C. Lee, K.-S.T.-H. Lim, Y.-E. Sung, A. Wieckowski, S.-K. Kim, Energy Environ. Sci. 5 (2012) 7521–7525.
[27] S.J. Hwang, S.-K. Kim, J.-G. Lee, S.-C. Lee, J.H. Jang, P. Kim, T.-H. Lim, Y.-E. Sung, S.J. Yoo, J. Am. Chem. Soc. 134 (2012) 19508–19511.
[28] C.-H. Cui, S.-H. Yu, Acc. Chem. Res. 46 (2013) 1427–1437.
[29] H.-H. Li, S. Zhao, M. Gong, C.-H. Cui, D. He, H.-W. Liang, L. Wu, S.-H. Yu, Angew. Chem. Int. Ed. 52 (2013) 7472–7476.
[30] H.-H. Li, C.-H. Cui, S. Zhao, H.-B. Yao, M.-R. Gao, F.-J. Fan, S.-H. Yu, Adv. Energy Mater. 2 (2012) 1182–1187.
[31] M. Shao, K. Shoemaker, A. Peles, K. Kaneko, L. Protsalio, J. Am. Chem. Soc. 132 (2010) 9253–9255.
[32] T. Cochell, W. Li, A. Manthiram, J. Phys. Chem. C 117 (2013) 3865–3873.
[33] T. Cochell, A. Manthiram, Langmuir 28 (2012) 1579–1587.
[34] H. Wang, R. Wang, H. Li, Q. Wang, J. Kang, Z. Lei, Int. J. Hydrogen Energy 36 (2011) 839–848.
[35] S.J. Hwang, S.J. Yoo, J. Shin, Y.-H. Cho, J.H. Jang, E. Cho, Y.-E. Sung, S.W. Nam, T.-H. Lim, S.-C. Lee, S.-K. Kim, Sci. Rep. 3 (2013) 1309.
[36] S. Beak, D. Jung, K.S. Nahm, P. Kim, Catal. Lett. 134 (2010) 288–294.
[37] F.M. Alamgir, Effect of surface-to-bulk atomic structure on surface electronic structure in multicomponent catalysts, 57th Annual Report on Research Under Sponsorship of The American Chemical Society Petroleum Research Fund. 2015.
[38] Y.D. Yin, R.M. Rioux, C.K. Erdonmez, S. Hughes, G.A. Somorjai, A.P. Alivisatos, Science 304 (2004) 711–714.
[39] Y. Zhang, C. Ma, Y. Zhu, R. Si, Y. Cai, J.X. Wang, R.R. Adzic, Catalysis Today 202 (2013) 50–54.
[40] J.X. Wang, C. Ma, Y. Choi, D. Su, Y. Zhu, P. Liu, R. Si, M.B. Vukmirovic, Y. Zhang, R.R. Adzic, J. Am. Chem. Soc 133 (2011) 13551–13557.